Propagation Characteristics of Surge Produced by Landslides

Hiroshi Takebayashi[1*], Masaharu Fujita[1], Tetsuro Kajihara[2]

[1] Disaster Prevention Research Institute, Kyoto University (Higashinoguchi, Shimomisu, Yokoouji, Fushimi, Kyoto 6128235, Japan)

[2] Graduate School of Engineering, Kyoto University (Kyoto daigaku-Katsura, Nishikyo-ku, Kyoto 615-8530 , Japan)

*Corresponding author. E-mail: takebayashi@sabom.dpri.kyoto-u.ac.jp

Propagation characteristics of surges in a straight channel with mild slope have been researched under small water discharge conditions by many researchers, because tsunami and tidal bores are observed near the coastal area. On the other hand, surges are also produced in mountainous rivers. It is considered that two landslides grasdfasdfsred in a curvature of the river and surges are produced by the upstream landslide in the Totsu River, Uguhara, Japan on Sep. 2011. The planar shape of the Totsu River in Uguhara is meandering and the bed slope is steep. Additionally, it is considered that the surges are propagated in upstream direction under large water discharge during a flood. In this study, propagation characteristics of surges produced by landslides in the mountainous river have been discussed by using flume tests and horizontal two dimensional numerical analysis. Results show that the transverse distribution of the water velocity and the reflection of the surges from the walls are small in a straight channel, but the transverse distribution of the water velocity is large in the meandering channel. Additionally, the reflection of the surges from the walls is large, because the propagation direction of the surge is not parallel to the walls. Hence, the surge in a meandering channel tends to be dispersed and the first surge has smaller value than that in a straight channel. The water impounded by the downstream landslide dam makes the propagation velocity of the surge induced by the upstream landslide dam faster. This results indicates the possibility that one landslide affects on the other landslides and causing more severe disasters.

Key words: surge, landslide, landslide dam, numerical analysis, meandering channel

1. INTRODUCTION

Typhoon TALAS went across the Japanese archipelago from Kochi Prefecture in Shikoku Island on Sep. 3 2011 to Hyogo Prefecture on Sep. 4 2011. The velocity of Typhoon TALAS was very slow. Typhoons around Japan rotates in the anticlockwise direction. Hence, the east side area of the Typhoons tends to have large damages, because precipitation increases. Kii peninsula located at the east side of the route of Typhoon TALAS and had a lot of precipitation for a long time. Total precipitation in the most parts of the Kii peninsula exceeded 1000mm. The total precipitation at Kamikitayama in Nara Prefecture was 2439mm.

During the heavy rain, many landslides occurred and landslides dams were formed. Plunge of failure masses into rivers produces surges. There is a possibility that the upstream propagation surge occur in the Totsu River at Uguhara, Totsugawa town, Nara, Japan and the surge attacked the Nagatono electric power plant.

Propagation characteristics of surges in a straight channel with mild slope have been studied under small water discharge conditions by many researchers, because tsunami and tidal bores are observed in rivers near the coastal area. On the other hand, surges are also produced in mountainous rivers. It is considered that surges are produced by landslides in the Totsu River, Uguhara, Japan on Sep. 2011. The planar shape of the Totsu River in Uguhara is meandering and the bed slope is steep. Additionally, it is considered that the surges are propagated in the upstream direction under large water discharge condition. In this study, propagation characteristics of surges produced by landslides in the mountainous river have been discussed by using flume tests and horizontal two dimensional numerical analysis.

2. TWO LANDSLIDES AT UGUHARA, TOTSUGAWA TOWN, JAPAN

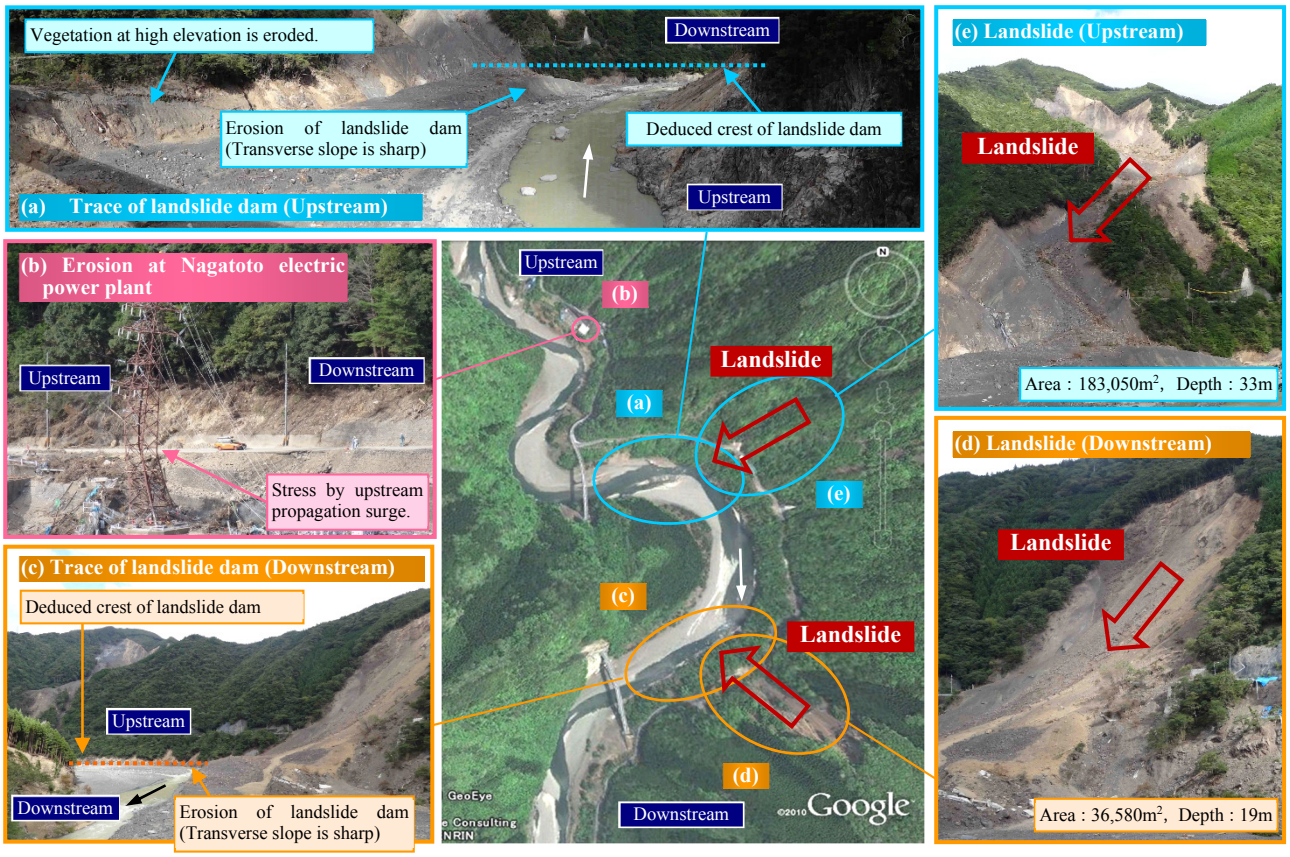

Fig. 1 Formation and erosion of landslide dam at the Totsu River in Nara Prefecture, Japan

Table 1 Hydraulic conditions

	Discharge (m^3/s)	Landslide dam	Channel shape
Case 1	0.00096	No	Meandering
Case 2	0.00096	Yes	Meandering
Case 3	0.00092	No	Straight
Case 4	0.00092	Yes	Straight
Case 5	2500	No	Meandering
Case 6	2500	Yes	Meandering

Two landslides occur at Uguhara, Ttsugawa town, Nara, Japan during the flood on Sep in 2011. The distance between the two landslides is 450m and locate in the same curvature of the Totsugawa River. It is considered that those landslides produced landslide dams and the dams were eroded during the flood. The precipitation during the flood was huge.

Fig. 1(a) and **(e)** shows the upstream landslide and the trace of the landslide dam. **Fig. 1 (c)** and **(d)** shows the downstream landslide and the trace of the landslide dam. The deduced height of the upstream landslide dam is higher than that of the downstream landslide dam, because of the difference of the produced sediment.

Nagatono electric power plant which is located at 1km upstream from the upstream landslide was damaged during the flood. The tower at the electric power plant was bent by the stress from the downstream. It is considered that the surge produced by the upstream landslide as shown in **Fig. 1 (a)** causes the stress, because the vegetation around the tower was fallen to the upstream direction. However, the electric power plant had been unmanned since 1982 and there is no eyewitness.

3. EXPERIMENT AND NUMERICAL ANALYSIS

3.1 Experimental flume

Fig. 2 shows the experimental flumes. The planar shapes of the fume are the meandering channel with sine-generated curve and the straight channel. The channel width of both channels is 20cm. The longitudinal slope along the channels is 1/100. The maximum meandering angle of the meandering channel is 60 degree. The surge is produced by the surge generation equipment as shown in **Fig. 3**. The

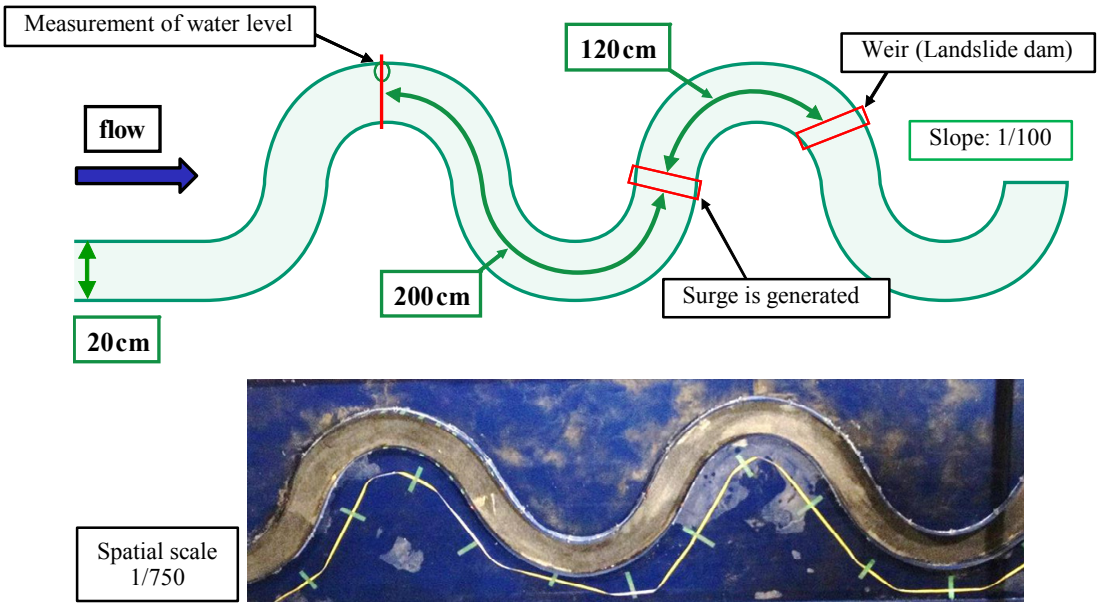

(a) Meandering channel

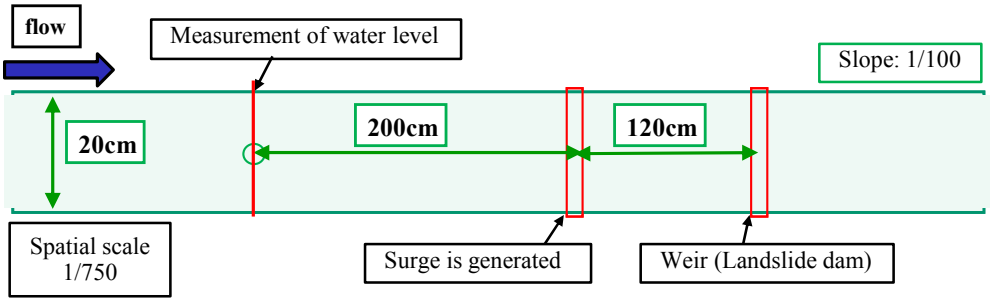

(b) Straight channel

Fig. 2 Channel geometry

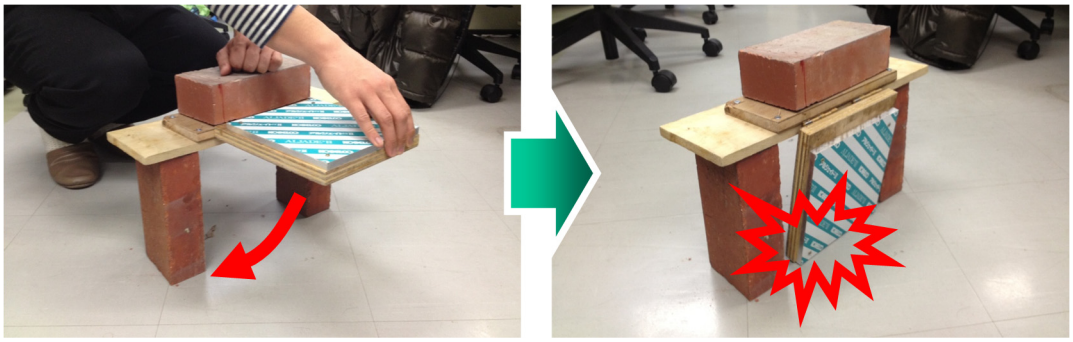

Fig. 3 Surge generation equipment

distance from the surge generation equipment to the measurement point of the water depth is about 200cm. The effect of the retained water by the downstream landslide dam on the surge propagation characteristics is discussed by setting the weir at 120cm downstream from the surge generation equipment.

2.2 Basic equations

Computation of water flow was performed using the governing equation for the horizontal two-dimensional flow averaged with depth. The equations are expressed in the boundary fitted orthogonal curvilinear coordinates. Mass conservation equation is as follows:

$$\frac{\partial}{\partial t}\left(\frac{z}{J}\right)+\frac{\partial}{\partial \xi}\left(\frac{hU}{J}\right)+\frac{\partial}{\partial \eta}\left(\frac{hV}{J}\right)=0 \qquad (1)$$

where, t is the time, z is the water surface level. Water depth is represented as h, U and V represent the contravariant depth averaged flow velocity on bed along ξ and η coordinates, respectively. These

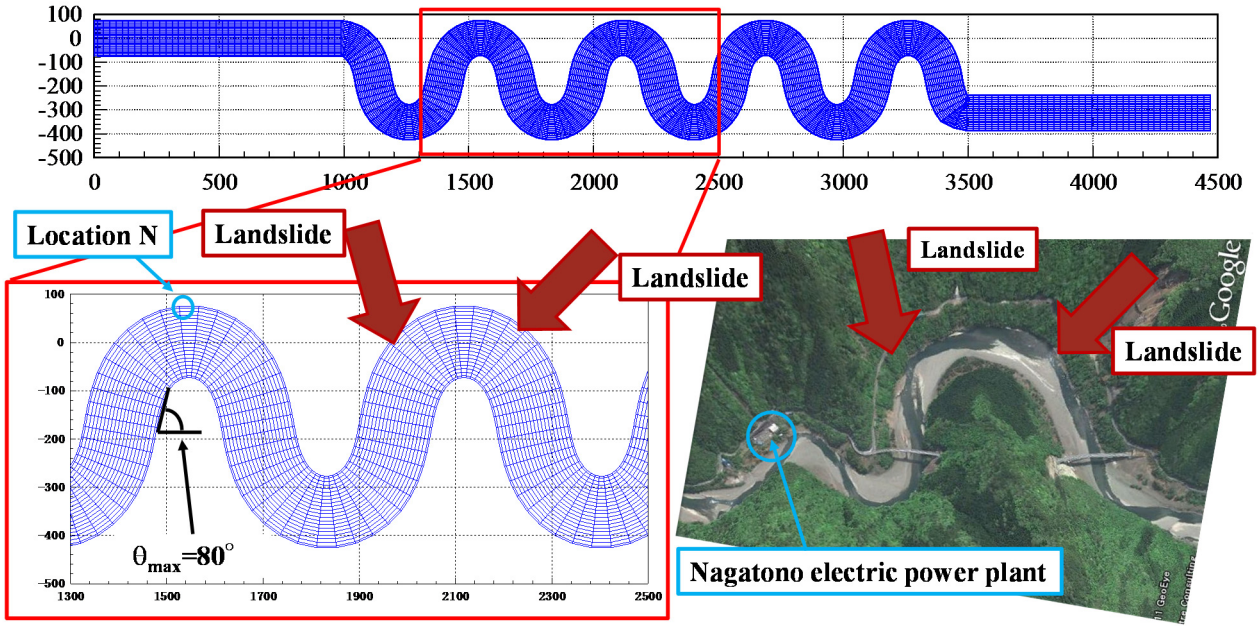

Fig. 4 Grids for numerical analysis

velocities are defined as

$$U = \frac{\partial \xi}{\partial x} u + \frac{\partial \xi}{\partial y} v \tag{2}$$

$$V = \frac{\partial \eta}{\partial x} u + \frac{\partial \eta}{\partial y} v \tag{3}$$

where, u and v represent depth averaged flow velocity on bed along x and y coordinates, respectively. Momentum equations of water are as follows.

$$\begin{aligned}
&\frac{\partial}{\partial t}\left(\frac{hU}{J}\right)+\frac{\partial}{\partial \xi}\left(U\frac{hU}{J}\right)+\frac{\partial}{\partial \eta}\left(V\frac{hU}{J}\right)\\
&-\frac{hu}{J}\left(U\frac{\partial}{\partial \xi}\left(\frac{\partial \xi}{\partial x}\right)+V\frac{\partial}{\partial \eta}\left(\frac{\partial \xi}{\partial x}\right)\right)\\
&-\frac{hv}{J}\left(U\frac{\partial}{\partial \xi}\left(\frac{\partial \xi}{\partial y}\right)+V\frac{\partial}{\partial \eta}\left(\frac{\partial \xi}{\partial y}\right)\right)\\
&=-gh\left(\frac{1}{J}\left(\left(\frac{\partial \xi}{\partial x}\right)^2+\left(\frac{\partial \xi}{\partial y}\right)^2\right)\frac{\partial z_s}{\partial \xi}\right.\\
&\qquad\left.+\frac{1}{J}\left(\frac{\partial \xi}{\partial x}\frac{\partial \eta}{\partial x}+\frac{\partial \xi}{\partial y}\frac{\partial \eta}{\partial y}\right)\frac{\partial z_s}{\partial \eta}\right)-\frac{\tau_{b\xi}}{\rho J}\\
&+\frac{1}{J}\left(\frac{\partial \xi}{\partial x}\right)^2\frac{\partial}{\partial \xi}\left(h\sigma_{xx}\right)+\frac{1}{J}\frac{\partial \xi}{\partial x}\frac{\partial \eta}{\partial x}\frac{\partial}{\partial \eta}\left(h\sigma_{xx}\right)\\
&+\frac{1}{J}\frac{\partial \xi}{\partial y}\frac{\partial \eta}{\partial x}\frac{\partial}{\partial \eta}\left(h\tau_{yx}\right)+\frac{1}{J}\frac{\partial \xi}{\partial y}\frac{\partial \xi}{\partial x}\frac{\partial}{\partial \xi}\left(h\tau_{yx}\right)\\
&+\frac{1}{J}\frac{\partial \xi}{\partial x}\frac{\partial \eta}{\partial y}\frac{\partial}{\partial \eta}\left(h\tau_{xy}\right)+\frac{1}{J}\frac{\partial \xi}{\partial x}\frac{\partial \xi}{\partial y}\frac{\partial}{\partial \xi}\left(h\tau_{xy}\right)\\
&+\frac{1}{J}\left(\frac{\partial \xi}{\partial y}\right)^2\frac{\partial}{\partial \xi}\left(h\sigma_{yy}\right)+\frac{1}{J}\frac{\partial \xi}{\partial y}\frac{\partial \eta}{\partial y}\frac{\partial}{\partial \eta}\left(h\sigma_{yy}\right)
\end{aligned} \tag{4}$$

$$\begin{aligned}
&\frac{\partial}{\partial t}\left(\frac{hV}{J}\right)+\frac{\partial}{\partial \xi}\left(U\frac{hV}{J}\right)+\frac{\partial}{\partial \eta}\left(V\frac{hV}{J}\right)\\
&-\frac{hu}{J}\left(U\frac{\partial}{\partial \xi}\left(\frac{\partial \eta}{\partial x}\right)+V\frac{\partial}{\partial \eta}\left(\frac{\partial \eta}{\partial x}\right)\right)\\
&-\frac{hv}{J}\left(U\frac{\partial}{\partial \xi}\left(\frac{\partial \eta}{\partial y}\right)+V\frac{\partial}{\partial \eta}\left(\frac{\partial \eta}{\partial y}\right)\right)\\
&=-gh\left(\frac{1}{J}\left(\frac{\partial \xi}{\partial x}\frac{\partial \eta}{\partial x}+\frac{\partial \xi}{\partial y}\frac{\partial \eta}{\partial y}\right)\frac{\partial z_s}{\partial \xi}\right.\\
&\qquad\left.+\frac{1}{J}\left(\left(\frac{\partial \eta}{\partial x}\right)^2+\left(\frac{\partial \eta}{\partial y}\right)^2\right)\frac{\partial z_s}{\partial \eta}\right)-\frac{\tau_{b\eta}}{\rho J}\\
&+\frac{1}{J}\frac{\partial \eta}{\partial x}\frac{\partial \xi}{\partial x}\frac{\partial}{\partial \xi}\left(h\sigma_{xx}\right)+\frac{1}{J}\left(\frac{\partial \eta}{\partial x}\right)^2\frac{\partial}{\partial \eta}\left(h\sigma_{xx}\right)\\
&+\frac{1}{J}\frac{\partial \eta}{\partial y}\frac{\partial \xi}{\partial x}\frac{\partial}{\partial \xi}\left(h\tau_{yx}\right)+\frac{1}{J}\frac{\partial \eta}{\partial y}\frac{\partial \eta}{\partial x}\frac{\partial}{\partial \eta}\left(h\tau_{yx}\right)\\
&+\frac{1}{J}\frac{\partial \eta}{\partial x}\frac{\partial \xi}{\partial y}\frac{\partial}{\partial \xi}\left(h\tau_{xy}\right)+\frac{1}{J}\frac{\partial \eta}{\partial x}\frac{\partial \eta}{\partial y}\frac{\partial}{\partial \eta}\left(h\tau_{xy}\right)\\
&+\frac{1}{J}\frac{\partial \eta}{\partial y}\frac{\partial \xi}{\partial y}\frac{\partial}{\partial \xi}\left(h\sigma_{yy}\right)+\frac{1}{J}\left(\frac{\partial \eta}{\partial y}\right)^2\frac{\partial}{\partial \eta}\left(h\sigma_{yy}\right)
\end{aligned} \tag{5}$$

where g is the gravitational acceleration, ρ is the water density. $\tau_{b\xi}$ and $\tau_{b\eta}$ represent the contravariant shear stress along ξ and η coordinates, respectively. These shear stresses are defined as

$$\tau_{b\xi} = \frac{\partial \xi}{\partial x}\tau_{bx} + \frac{\partial \xi}{\partial y}\tau_{by} \tag{6}$$

$$\tau_{b\eta} = \frac{\partial \eta}{\partial x}\tau_{bx} + \frac{\partial \eta}{\partial y}\tau_{by} \quad (7)$$

where, τ_x and τ_y are the shear stress along x and y coordinates, respectively as follows.

$$\tau_x = \tau_b \frac{u_b}{\sqrt{u_b^2 + v_b^2}} \quad (8)$$

$$\tau_y = \tau_b \frac{v_b}{\sqrt{u_b^2 + v_b^2}} \quad (9)$$

$$\frac{\tau_b}{\rho} = u_*^2 \quad (10)$$

$$u_*^2 = \frac{n_m^2 g}{R^{1/3}}\left(u^2 + v^2\right) \quad \text{or} \quad u_*^2 = \frac{u^2 + v^2}{\left(6 + 2.5\ln\frac{h}{k_s}\right)^2} \quad (11)$$

where, u_* is the friction velocity, n_m is the Manning's roughness coefficient, R is the hydraulic radius, k_s is the roughness height. u_b and v_b represent velocity near the bed surface along x and y coordinates, respectively. Velocities near the bed are evaluated using curvature radius of streamlines as follows.

$$u_b = u_{bs}\cos\alpha_s - v_{bs}\sin\alpha_s \quad (12)$$

$$v_b = u_{bs}\sin\alpha_s + v_{bs}\cos\alpha_s \quad (13)$$

$$u_{bs} = 8.5u_* \quad (14)$$

$$v_{bs} = -N_*\frac{h}{r}u_{bs} \quad (15)$$

where, $\alpha_s = \arctan\left(v/u\right)$, N_* is 7.0 (Engelund, 1974) and r is the curvature radius of stream lines obtained by depth integrated velocity field as follows (Shimizu and Itakura, 1991).

$$\frac{1}{r} = \frac{1}{\left(u^2 + v^2\right)^{3/2}} \left\{u\left(u\frac{\partial v}{\partial x} - v\frac{\partial u}{\partial x}\right) + v\left(u\frac{\partial v}{\partial y} - v\frac{\partial u}{\partial y}\right)\right\} \quad (16)$$

σ_{xx}, σ_{yy}, τ_{xy} and τ_{yx} are turbulence stresses as follows.

$$\sigma_{xx} = 2\nu\frac{\partial u}{\partial x} \quad (17)$$

$$\sigma_{yy} = 2\nu\frac{\partial v}{\partial y} \quad (18)$$

$$\tau_{xy} = \tau_{yx} = \nu\left(\frac{\partial v}{\partial x} + \frac{\partial u}{\partial y}\right) \quad (19)$$

$$\nu = \frac{\kappa}{6}u_* h \quad (20)$$

where, ν is the coefficient of kinematic eddy viscosity, κ is the Karman constant.

3.3 Hydraulic conditions

Table 1 shows the hydraulic conditions of flume tests and numerical analysis. The location of the production of surges (location of the upstream landslide) is shown in **Fig 2**. Furthermore, one more landslide is considered under Cases 2, and 4 and produces landslide dam in the downstream area of upstream landslide. In Cases 2, and 4, water impounded in the upstream area of the downstream landslide dam and the upstream landslide sediment flows into the deposited water. The distance between the downstream landslide dam and the upstream landslide is 1.2m and the distance between the upstream landslide to the measurement instrument of water surface level is 2m. In the numerical analysis, the surge is produced by uplifting the bed rapidly. The bed is uplifted equally in the transvers direction. The longitudinal geometry of the upstream landslide dam is triangle and the height of its crest is 5.5cm. The uplift speed of the bed is 11cm/s. The downstream landslide dam geometry is considered as an initial bed geometry in the calculation. In the experiment, a weir is set as the downstream landside dam.

The hydraulic conditions of Cases 5 and 6 are determined in reference to the hydraulic conditions of the Totsu River. **Fig. 4** shows the grids of numerical analysis of Cases 5 and 6. The planar shape of the calculation domain is the meandering channel with sine-generated curve. The channel width is 150m, the bed slope along the channel is 1/100, and the maximum meandering angle is 80 degree. Treatments of the surge and landslide in Case 5 and 6 are the same as those in Case 2, and 4. However, the height of the crest of the landslide dams is 9m and the uplift speed of the bed is 1m/s.

3. RESULTS AND DISCUSSION

Fig. 5 shows the temporal change of water surface elevation obtained by the flume tests (Cases 1, 2, 3, and 4). As shown in **Fig. 5**, the surge is propagated to the upstream direction and the water depth is increased rapidly, when the surge is arrived.

The difference of the propagation velocity of the surge between Cases 1 and 2 is large. When the water deposition due to the downstream landslide dam is considered (Case 2), the propagation velocity of the surge in upstream direction is 6s and faster than that without landslide dam (Case 1). The propagation velocity is affected by the water depth to the power of 0.5 and the velocity in longitudinal direction. When the water depth is deep and the velocity in downstream direction is small, the propagation velocity of surge in upstream direction becomes

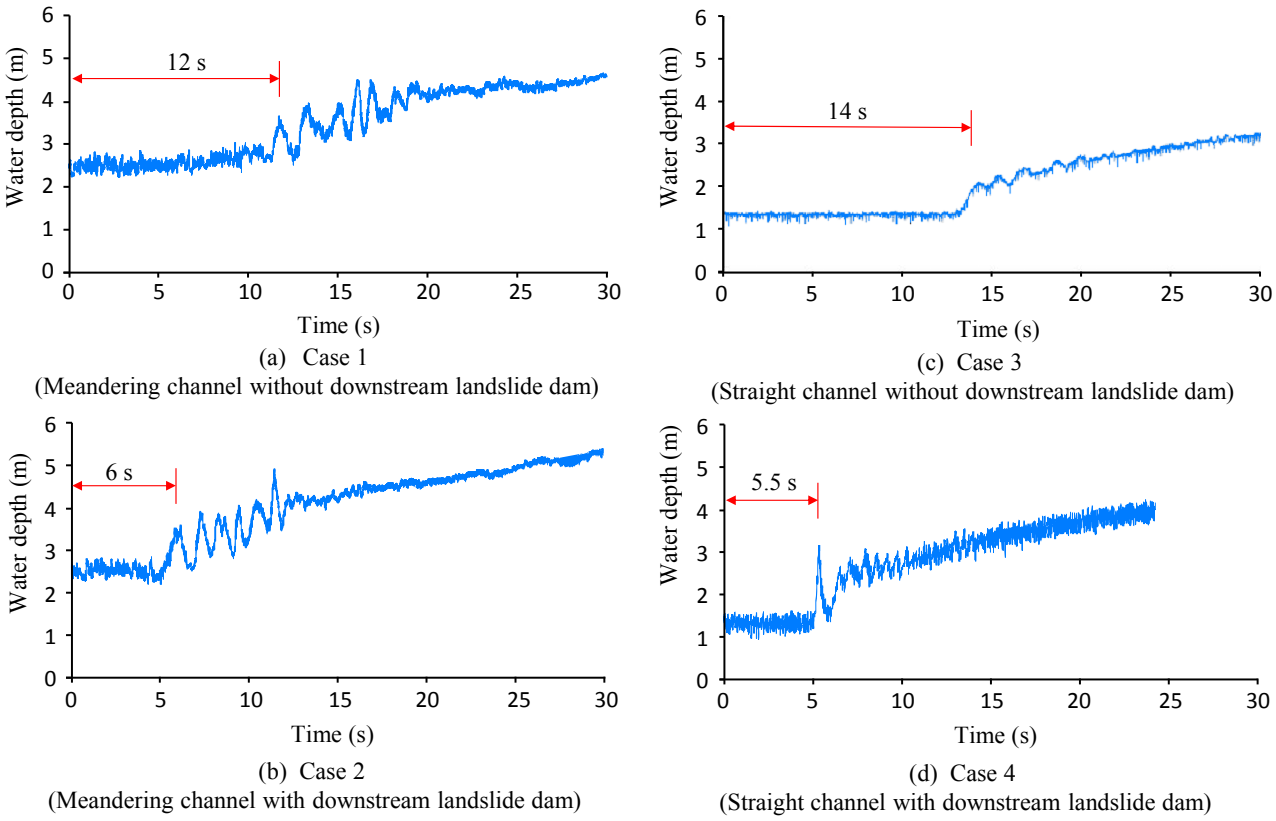

Fig. 5 Temporal change of water depth at 2m upstream from surge generation cross-section (flume tests)

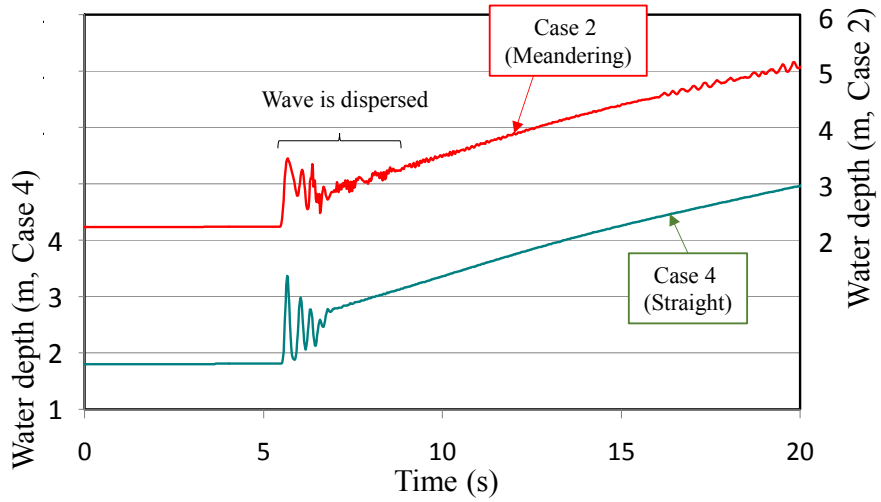

Fig. 6 Temporal change of water depth at 2m upstream from surge generation cross-section (numerical analysis)

faster. Hence, the propagation velocity of the surge in Case 2 is faster than that in Case 1.

The difference of the propagation velocity between Cases 2 and 4 is small. However, the dispersion characteristics of the surges are different. The surge in the straight channel (Case 4) has one large peak. On the other hand, the surges are dispersed in the meandering channel (Case 2) and the first surge in the meandering channel has smaller value than that in Case 4. In a straight channel, the transverse distribution of the water velocity and the reflection of the surges from the walls are small. On the other hand, as shown in **Fig. 8**, the transverse distribution of the water velocity is fast in the meandering channel. Additionally, the reflection of the surges from the walls is large in the meandering channel, because the propagation direction of the surge is not parallel to the walls. As a result, the surges are dispersed in Case 2. This is the important characteristics of the propagation characteristics of surges in meandering channels.

Fig. 6 shows the temporal change of the water

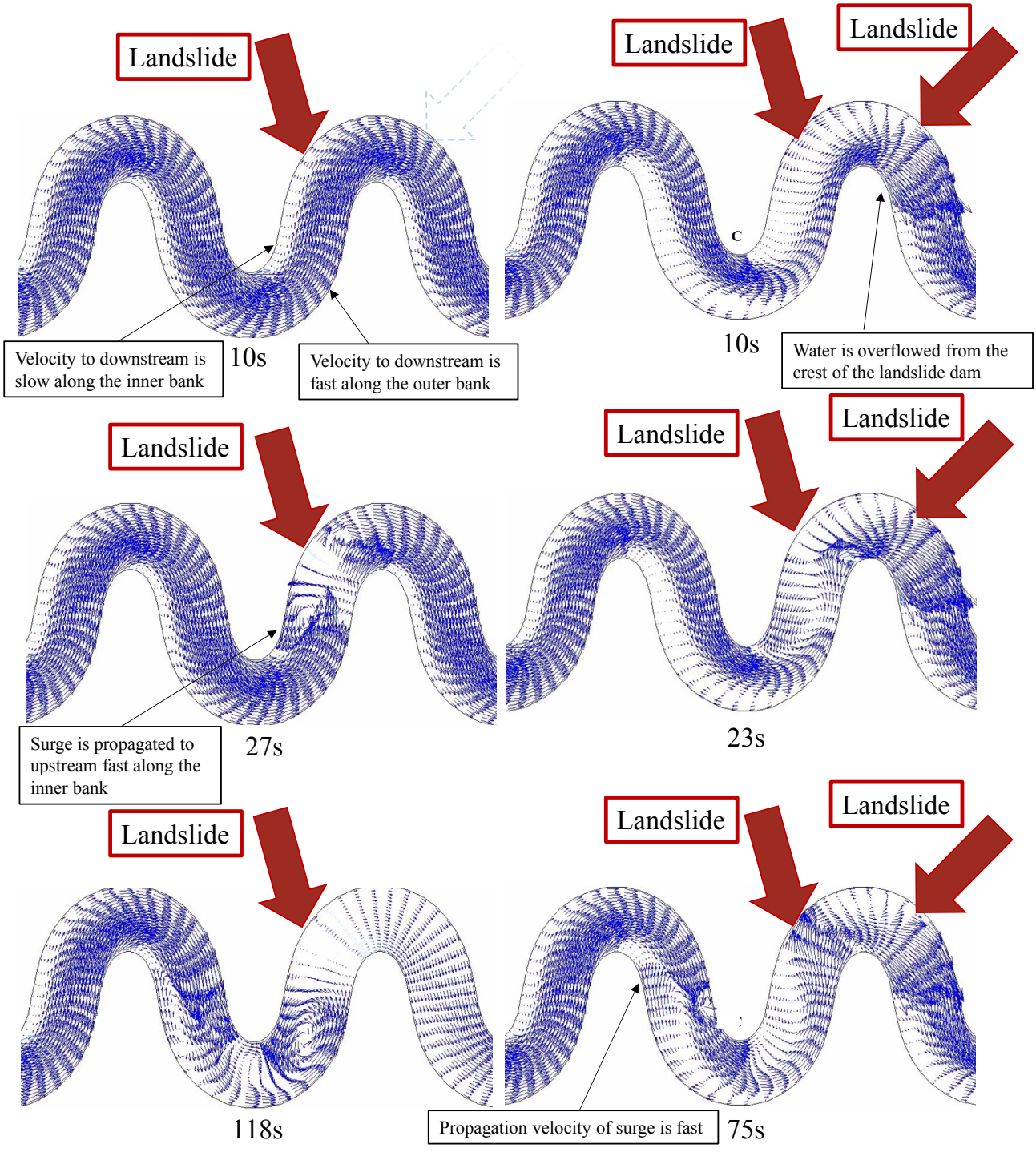

(a) Case 5 (b) Case 6

Fig. 7 Temporal change of depth integrated water velocity (numerical analysis, Case 5 and Case 6)

depth at 2m upstream from the surge generation point in Cases 2 and 4. There are some differences between the results of the numerical analysis and the flume tests. However, the tendencies that the water depth of the first surge in Case 2 is smaller than that in Case 4 and the surge tends to be dispersed are reproduced.

Fig. 7 (a) shows the temporal change of the horizontal distribution of depth integrated water velocity in Case 5. As shown in **Fig. 7 (a)**, the water velocity is smaller near the inner bank in the downstream of the curvature than that near the outer bank and the water velocity is fast near the outer bank in the downstream of the curvature. The transvers distribution of the longitudinal water velocity in downstream direction affects on the upstream propagation velocity of the surge. The surge propagates faster in the upstream direction near the inner bank where the water velocity in the dow

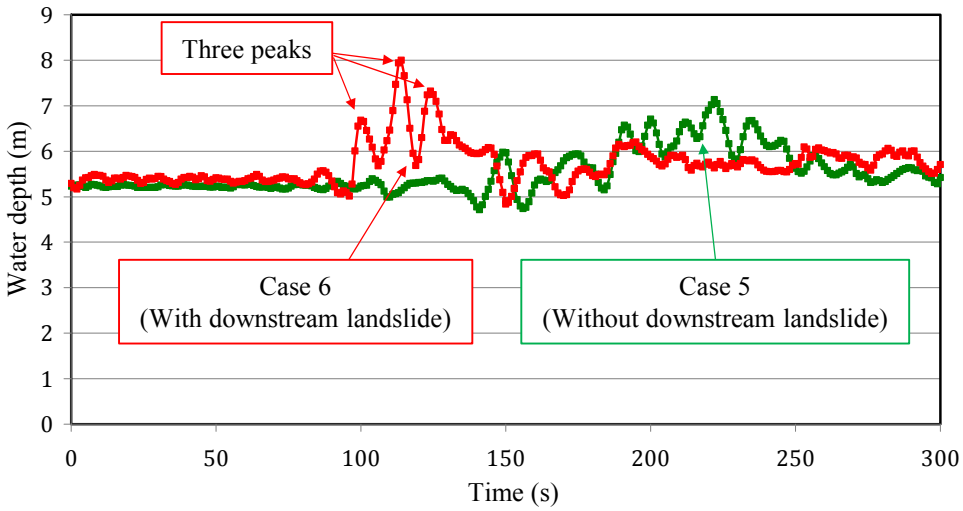

Fig. 8 Temporal change of water depth at Location N (numerical analysis, Cases 5 and 6)

Table 2 Hydraulic conditions

	Propagation time (s)	Propagation velocity (m/s)	Maximum wave height
Case 1	150	5.3	Meandering
Case 2	100	8.0	Meandering

nstream direction is smaller than that near the outer bank. Additionally, the surge is reflected along sidewalls. Hence, the surge is dispersed and three clear peaks of surges are formed as shown in **Fig. 8**.

The propagation velocity of surges in a straight channel is uniform in transverse direction and the dispersion of the surge is smaller. Hence the surge in a straight channel can be discussed by use of one dimensional model. However, when the characteristics of the surge in a meandering channel is discussed, horizontal two dimensional model has some advantages.

Fig. 7 (b) shows the temporal change of the horizontal distribution of depth with water velocity in Case 6. As shown in **Fig. 7 (b)**, the longitudinal water velocity in downstream direction becomes slower because of the back water effect by the downstream landslide dam.

Fig. 8 shows the temporal change of the water depth at Location N, as shown in **Fig. 4**, in Cases 5 and 6. Table 2 shows the propagation characteristic vales of surges. The maximum surge wave height is 1.9m and the propagation velocity is 5.3m/s in Case 5. On the other hand, the maximum surge wave height in Case 6 is 2.8m and the propagation velocity of the surge in Case 6 is 8.0m/s. As described before the propagation velocity of the surge is affected by the water depth to the power of 0.5 and the water velocity. In Case 6, the water depth is deeper and the longitudinal water velocity in the downstream direction is smaller than those in Case5. Hence the surge in Case 6 is propagated faster.

This results indicates the possibility that one landslide affects on the other landslides and cause more severe disasters.

4. CONCLUSIONS

Propagation characteristics of surges produced by landslides in the mountainous river have been discussed by use of flume tests and horizontal two dimensional numerical analysis. Obtained results are as follows:

(1) The propagation velocity of the surge is affected by the water depth to the power of 0.5 and the water velocity. When the water depth is deep and the water velocity in downstream direction is small, the propagation velocity of surge in upstream direction becomes faster. Hence, the water deposition by the downstream landslide dam makes the propagation velocity of the surge by the upstream landslide dam faster. This results indicates the possibility that one landslide affects on the other landslides and cause more severe disasters.

(2) In a straight channel, the transverse distribution of the water velocity and the reflection of the surges from the walls are small. On the other hand, the transverse distribution of the water velocity is large in the meandering channel. Additionally, the reflection of the surges from the walls is large, because the propagation direction of the surge is not parallel to the walls. Hence, the surge in a meandering channel tends to be dispersed and the first surge has smaller value.

ACKNOWLEDGMENT: This research is funded by Kinki Construction Association Research Grand (Representative: Hiroshi Takebayashi), Grant-in-Aid for Scientific Research for young researchers (B) (Representative: Hiroshi Takebayashi), RIC Research Fund (Representative: Hiroshi Takebayashi), Disaster Science Research Institute Corporative Research (Civil engineering and Co-Technology Consultants Co.,Ltd.), Natural Disaster Research Council Research Grand.

REFERENCES

Engelund, F. (1974): Flow and bed topography in channel bends. Jour. of Hy. Div. ASCE, Vol. 100, No. HY11, pp. 1631-1648.

Shimizu,Y. and Itakura,T. (1991): Calculation of flow and bed deformation with a general non-orthogonal coordinate system, Proc. of XXIV IAHR Congress, Madrid, Spain, C-2, pp.41-48.